Quantum-Chemical Investigation of the Electroabsorption Spectra of Directly *Meso*−*Meso*-Linked Porphyrin Arrays: Essential Role of Charge-Transfer Excited States Accidentally Overlapping with Soret Bands

Yoichi Matsuzaki*

Advanced Technology Research Laboratories, Nippon Steel Corporation, 20-1 Shintomi, Futtsu, Chiba 293-8511, Japan

Atsushi Nogami

Department of Environmental Space Design, The University of Kitakyushu, 1-1, Hibikino, Wakamatsu-ku, Kitakyushu, Fukuoka 808-0135, Japan

Yuji Iwaki and Nobuhiro Ohta

Research Institute for Electronic Science, Hokkaido University, Sapporo 060-0812, Japan

Naoya Yoshida, Naoki Aratani, and Atsuhiro Osuka*

Department of Chemistry, Kyoto University, Kyoto 606-8502, Japan

Kazuyoshi Tanaka

Department of Molecular Engineering, Graduate School of Engineering, Kyoto University, Nishikyo-ku, Kyoto 615-8510, Japan

Received: August 20, 2004; In Final Form: November 2, 2004

The electroabsorption (EA) spectra of directly *meso*−*meso*-linked porphyrin arrays (**Z*n***, $n = 1-3$) have been investigated by means of the sum-over-states (SOS) approach at the INDO/S-SCI level theory. The experimental EA spectra of **Z*n*** ($n \geq 2$) exhibit an unusual second-derivative line shape at the exciton split low-energy B_x band in contrast to the first-derivative spectrum of **Z1**, which is readily ascribed to a quadratic Stark shift of the B (Soret) band. Although the second-derivative line shape is usually attributed to a difference in the permanent dipole moment ($\Delta\mu$) between the ground and excited states, it should be vanishing for **Z*n*** due to their essentially D_{2d} or D_{2h} symmetry. As pointed out in our previous studies, the interporphyrinic charge-transfer (CT) excited states are accidentally overlapping with the excitonic B bands and the present calculations reveal that the B_x state is strongly coupled via a transition dipole moment with two such CT states. These situations give rise to a quadratic Stark effect on the B_x band that is intermediate between Stark shift (first derivative) and Stark broadening (second derivative), and play a central role in establishing the anomalous second derivative nature of the EA spectrum. Moreover, based on the comparison between the theoretical and experimental spectra, there must be an additional factor that further enhances the second derivative nature of the EA spectrum of porphyrin arrays. Discussions on this issue including the preliminary investigations on the role of solvent (PMMA)-induced asymmetry are also presented.

I. Introduction

In recent years, a variety of porphyrin-based supramolecules have been developed primarily to mimic the photosynthetic reaction centers and light harvesting complexes[1] and further to obtain ideally suited properties for applications in molecular photonic and electronic devices.[2] The multiporphyrin systems are quite promising candidates for molecular devices since the optical and redox properties of porphyrins can be finely tuned by their chemical modifications and these pigments can be arranged into various architechtures either by covalent or noncovalent bonds. The huge variation in these supramolecules also spurs considerable attention on their structure−property relationship regarding many factors such as interporphyrin distance, orientation, and the electronic property of a linker which strongly affect their optical and electrical properties.

The directly *meso*−*meso*-linked Zn^{II}-porphyrin arrays, **Z*n*** (Figure 1), have been successfully synthesized up to $n = 128$ by repeated Ag(I)-salt-promoted dimerization reaction.[3,4] They maintain an orthogonal conformation between the neighboring porphyrin units with small conformational heterogeneity, thus offering a good opportunity for a systematic study on structure−property relationship. In their linear absorption spectra shown in Figure 2, the B (Soret) band is split into the low-energy B_x band and the high-energy degenerate B_{yz} band (the subscripts denote the direction of transition dipole moment under the axis definition indicated in Figure 1). Along with an increasing number of porphyrin subunits, the B_x band is systematically

* To whom all the correspondence should be addressed.

10.1021/jp040570b CCC: $30.25
Published on Web 01/04/2005

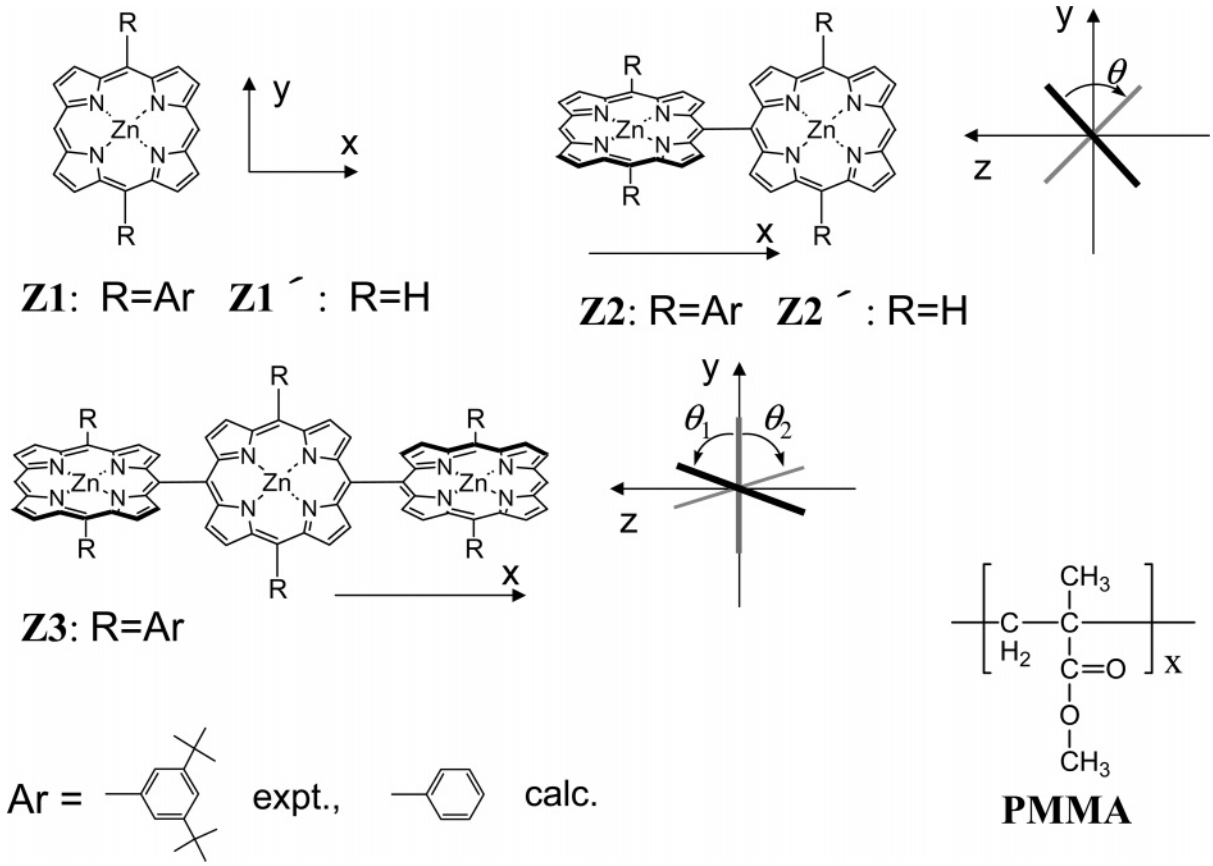

Figure 1. Chemical structure and axis definition for the porphyrin arrays investigated in this work. The porphyrin arrays are doped into a poly(methyl methacrylate) (PMMA) film in the experiments.

red-shifted due to the interaction between transition dipole moments (exciton coupling[5]) on adjacent subunits. On the other hand, the position of the B_{yz} band remains nearly unchanged from that of the monomer since the exciton coupling vanishes in this case due to the orthogonal conformation between neighboring porphyrins. The ample interchromophoric interactions as well as the small conformational disorder established by the direct linkage make these arrays an excellent photonic wire that transmits singlet excitation energy rapidly to the energy acceptor.[6]

The close proximity of adjacent porphyrin units in **Z*n*** also gives rise to rich electronic spectra in their B-band region due to the accidental overlap of interporphyrinic charge-transfer (CT) bands as has been pointed out in our molecular orbital studies on **Z2′**[7] as well as the *meso*−*meso*, *β*−*β*, *β*−*β* triply linked porphyrin arrays **T*n***.[8,9] Note that these CT states are represented by a 1:1 combination of oppositely directed charge-transfer transitions as a result of the symmetric molecular structure of **Z*n*** and hence carry no net transfer of charge. The unique absorption spectra for the strapped derivative of **Z2** (the interporphyrin dihedral angle is systematically controlled by changing the length of the strapping chain: $-O-(CH_2)_n-O-$) as well as the excited-state relaxation dynamics and the resonance Raman spectra of **T*n*** arrays have been successfully explained by taking account of these CT states.[7−9] In the present study, we focus on the electroabsorption (EA) spectra of **Z*n***[10] since they also exhibit anomalous features which hardly can be ascribed to an ordinary Stark shift of either B_x or B_{yz} band indicating a contribution from these CT states.

The EA spectroscopy is a highly sensitive and informative tool for studying the excited-state spectrum probing also the dipole-forbidden states of conjugated molecules and polymers responsible for their large nonlinear optical (NLO) responses.[11,12] As displayed in Figure 2, the EA spectra have been measured on **Z*n*** ($n = 1-4$) doped in a poly(methyl methacrylate) (PMMA, Figure 1) film.[10] The EA spectrum of **Z1** is nearly proportional to the first derivative of the B-band, which can be readily interpreted as a quadratic Stark shift due to the change in polarizability ($\Delta\alpha$) for the B state relative to the ground state. In contrast, the EA spectra of **Z*n*** ($n \geq 2$) exhibit a remarkable contribution from the second derivative of their B_x band as is clearly detected for **Z3** and **Z4**. The second-derivative EA signal arises from a field-induced broadening of the absorption spectrum and is usually connected with a difference in the permanent dipole moment ($\Delta\mu$) between the ground and excited states.[11] Although $\Delta\mu$ might be provided by a photoinduced charge transfer along the porphyrin array, such a mechanism cannot be totally accepted since the permanent dipole moment should be vanishing in **Z*n*** due to their essentially D_{2d} (even n) or D_{2h} (odd n) symmetry. A similar feature for the centrosymmetric system has been pointed out on the film sample of polyacetylene[13] and polydiacetylene[14] and has been interpreted as a linear Stark shift due to $\Delta\mu$ arising from disorder-induced asymmetry of polymer segments.[14] On the other hand, it is noteworthy that the second-derivative profile can emerge even for an ideally symmetric system ($\Delta\mu = 0$) via the $\Delta\alpha$ mechanism, if the energy gap between strongly coupled dipole-allowed and dipole-forbidden excited states is comparable with their line widths, i.e., "the quadratic Stark broadening".[15,16] In this paper, we show that this condition is nearly satisfied by **Z*n*** as a result of the accidental degeneracy of the B_x and CT states.

The origin of the EA signal around the B_{yz} band is also complicated since it is gradually red-shifted upon an increase

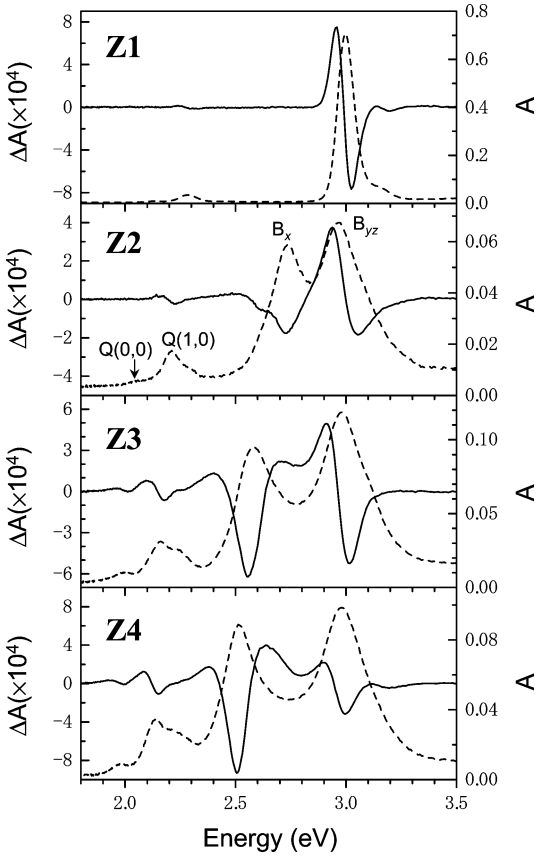

Figure 2. Experimental electroabsorption spectra of porphyrin monomer **Z1** and *meso*−*meso*-linked porphyrin arrays from **Z2** to **Z4** in a PMMA polymer film observed with a field strength of 0.75 MV cm^{-1} (solid lines), together with the linear-absorption spectra (dashed lines).

in the number of porphyrin units despite the essentially unchanged position of the corresponding linear absorption band. All of these features indicate a mechanism specific to multiporphyrin arrays in providing their electrooptic responses. To reveal the influence of interchromophoric CT transitions on the NLO responses of porphyrin arrays, we apply herein the INDO/S molecular orbital (MO) calculations as in our previous studies.

II. Computational Methods

The ground-state geometries of porphyrin systems were optimized by using the B3LYP hybrid density-functional theory as implemented in the Gaussian98 suite of programs.[17] The basis set used is the 6-31G[18] set for carbon, nitrogen, and hydrogen atoms, and Huzinaga's (14s8p5d) set contracted to [5s3p2d] for Zn.[19] The molecular symmetry of **Z1′** (Zn^{II}-porphin) was assumed to be D_{4h} while that of **Z1** was reduced from D_{2h} to D_2 due to the nonorthogonal orientation of attached phenyl groups with respect to the porphyrin plane (the optimized dihedral angle is 66.2°). A variable dihedral angle (θ) between adjacent porphyrin units as defined by $C_\alpha-C_{meso}-C_{meso}-C_\alpha$ is taken into account for the porphyrin dimers and trimers since the energy minimum is rather shallow around $\theta = 90°$.[7] For a given θ, we have optimized all the other geometrical parameters under the following symmetry constraints. The molecular symmetry of **Z2′** is D_{2d} when $\theta = 90°$, while it is reduced to D_2 at $\theta < 90°$. For every system of **Z2** and **Z3**, the molecular symmetry was assumed to be D_2 by keeping $\theta_1 = \theta_2$ in the latter (Figure 1); even in the case of $\theta_1 \neq \theta_2$ (symmetry is reduced to C_2), the induced dipole moment should be less significant since the net charge transfer between adjacent porphyrin units is nearly prohibited. The optimized *meso*−*meso* bond length of 1.510 Å for **Z2** is in sufficient agreement with that of 1.51 Å found in the X-ray structure of both Cu^{II}-diporphyrin[7] and Zn^{II}-porphyrin dimer and trimer.[20]

The electronic excited states of porphyrin systems have been calculated by the singles excited configuration interaction (SCI) method on the basis of the intermediate neglect of differential overlap model for spectroscopy (INDO/S) Hamiltonian.[21] The two-center Coulomb interactions were evaluated by the Nishimoto−Mataga formula.[22] All of the one-electron levels are considered in the SCI expansion taking advantage of the molecular symmetry to reduce the size of the Hamiltonian matrix. The Cartesian coordinate system for the SCI calculation is depicted in Figure 1, where the *x*, *y*, and *z* axes are set to the C_2 axes under the D_2 point group.

To characterize each excited state in terms of charge-transfer (CT) nature, we calculate the charge-transfer probability $\mathbf{P}_{e-h}$ on the basis of the SCI transition density matrix ρ^{ge}:[23]

$$P_{e-h}(r,s) = (\rho^{ge}_{rs})^2/2 \tag{1}$$

which represents the probability of simultaneously finding an electron at the *r*th atomic orbital (AO) and a hole at the *s*th AO.

Since the magnitude of EA exhibits a quadratic field dependence in all the systems, their EA spectra can be properly simulated by the frequency dispersion of $\mathrm{Im}\chi^{(3)}(-\omega;\omega,0,0)$. In the present study, we calculate the corresponding molecular second hyperpolarizability $\gamma(-\omega;\omega,0,0)$ by means of the sum-over-states (SOS) approach on the basis of INDO/S-SCI calculated transition energies and transition dipole moments. We start with the general SOS expression derived by Orr and Ward:[24]

$$\gamma_{abcd}(-\omega_\sigma;\omega_1,\omega_2,\omega_3) = \frac{e^4}{6\hbar^3}P(b,c,d;\omega_1,\omega_2,\omega_3)\sum_{l,m,n\neq g}\times \left\{\frac{\langle g|\mu_a|l\rangle\langle l|\bar{\mu}_d|m\rangle\langle m|\bar{\mu}_c|n\rangle\langle n|\mu_b|g\rangle}{(\Omega_{lg}-\omega_\sigma)(\Omega_{mg}-\omega_1-\omega_2)(\Omega_{ng}-\omega_1)} + \frac{\langle g|\mu_d|l\rangle\langle l|\bar{\mu}_a|m\rangle\langle m|\bar{\mu}_c|n\rangle\langle n|\mu_b|g\rangle}{(\Omega^*_{lg}+\omega_3)(\Omega_{mg}-\omega_1-\omega_2)(\Omega_{ng}-\omega_1)} + \frac{\langle g|\mu_b|l\rangle\langle l|\bar{\mu}_c|m\rangle\langle m|\bar{\mu}_a|n\rangle\langle n|\mu_d|g\rangle}{(\Omega^*_{lg}+\omega_1)(\Omega^*_{mg}+\omega_1+\omega_2)(\Omega_{ng}-\omega_3)} + \frac{\langle g|\mu_b|l\rangle\langle l|\bar{\mu}_c|m\rangle\langle m|\bar{\mu}_d|n\rangle\langle n|\mu_a|g\rangle}{(\Omega^*_{lg}+\omega_1)(\Omega^*_{mg}+\omega_1+\omega_2)(\Omega^*_{ng}+\omega_\sigma)}\right\} \tag{2}$$

where *a*, *b*, *c*, and *d* correspond to the molecular axes *x*, *y*, and *z*; ω_1, ω_2, and ω_3 represent the applied field frequency; $\omega_\sigma = \omega_1 + \omega_2 + \omega_3$ is the polarization-response frequency; *l*, *m*, and *n* label the excited states and *g* the ground state; μ_a is the *a*th component of the dipole operator ($\bar{\mu}_a = \mu_a - \langle g|\mu_a|g\rangle$); $\Omega_{lg} \equiv \omega_{lg} - i\Gamma_l$ with ω_{lg} the transition frequency from states *g* to *l* and Γ_l the broadening parameter of excited state *l*; and *P* stands for a simultaneous permutation of (*b*,*c*,*d*) and (ω_1,ω_2,ω_3) in an equivalent way. Note that we keep only the first term in the complete expression given by eq 43c of ref 24 since the second term should be excluded within the SCI scheme to guarantee the size extensivity of γ.[25,26] The SCI technique can properly reproduce the electroabsorption and third-harmonic generation (THG) spectra of π-conjugated polymers,[27,28] while an inclusion of higher excitations is required to obtain a correct two-photon absorption spectrum.[28]

TABLE 1: Transition Properties and Electronic Structures of Q and B Bands of Z1′ and Z1 As Obtained from INDO/S-SCI Calculations

band[a]	state[b]	ΔE (eV)[c]	f[d]	W_4 (%)[e]
		Z1′		
Q	$1E_u$	1.84 (2.18)	0.059 (0.005)	96.8
B	$2E_u$	3.22 (3.13)	2.102 (0.98)	93.2
		Z1		
Q_y	$1B_{2u}$	1.80 (2.14)	0.019	96.4
Q_x	$1B_{3u}$	1.81	0.014	96.5
B_y	$2B_{2u}$	3.06 (3.00)	2.784	93.0
B_x	$2B_{3u}$	3.10	2.010	93.8

[a] The subscript indicates the orientation of the transition dipole moment (see Figure 1 for the axis definition). [b] The excited states of **Z1** are indicated by the D_{2h} notation. [c] Excitation energy. Listed in parentheses are the experimental values taken from ref 29 for **Z1′** and ref 3 for **Z1**. [d] Oscillator strength. The experimental values taken from ref 29 are listed in parentheses. [e] The weight of the transitions within four orbitals in the SCI wave function.

On the basis of eq 2, the EA spectrum can be simulated by $\mathrm{Im}\gamma_s(-\omega;\omega,0,0)$ in which

$$\gamma_s = \frac{1}{15}\sum_{a,b}(\gamma_{aabb} + \gamma_{abba} + \gamma_{abab}) \tag{3}$$

provides an orientationally averaged response. As will be demonstrated later, the EA spectra for the present systems are sufficiently reproduced by taking only the triply resonant terms arising from the first term in eq 2 and including a few tensor components:

$$\gamma_{aabb}(-\omega;\omega,0,0) = \frac{e^4}{3\hbar^3}\sum_{l,m,n\neq g}\times \frac{\langle g|\mu_a|l\rangle\langle l|\bar{\mu}_b|m\rangle\langle m|\bar{\mu}_b|n\rangle\langle n|\mu_a|g\rangle}{(\omega_{lg}-\omega-i\Gamma_l)(\omega_{mg}-\omega-i\Gamma_m)(\omega_{ng}-\omega-i\Gamma_n)} \tag{4}$$

Note that $\mathrm{Im}\gamma_{aabb}(-\omega;\omega,0,0)$ represents the modulation of absorption along the *a* direction induced by a static electric field applied in the *b* direction (F_b). The simple expression given by eq 4 is useful in elucidating the essential excited states responsible for the characteristic EA signal. For instance, if the quadratic Stark shift of the "B" state (polarized along *a*) is dominated by its electronic coupling with the "A" state as mediated by F_b, this situation can be noted by a large contribution from the $l = n =$ B and $m =$ A term of eq 4. In the SOS calculation of γ either by eq 2 or 4, the lowest 300 excited states were included to obtain a well-converged EA spectrum. The linear polarizabilities $\alpha_s(-\omega;\omega)$ ($\alpha_s = (\alpha_{xx} + \alpha_{yy} + \alpha_{zz})/3$) were also calculated by the SOS scheme[24] to simulate the linear absorption spectra by $\mathrm{Im}\alpha_s$. The broadening parameter (Γ) was set to 0.09 eV for all the excited states on the basis of the best fit to the experimental B_x band with which we are mainly concerned in this study.

III. Results and Discussion

EA Spectra of Porphyrin Monomers. The Q- and B-band transition energies and oscillator strengths for **Z1′** (Zn^{II}-porphin) and **Z1** are listed in Table 1 as obtained by the INDO/S-SCI calculations. For both systems, the calculated B-band energies are in good agreement with the experiments,[3,29] while the Q-band transitions are systematically underestimated. The overestimation of oscillator strength for the B band is well-known to be a usual feature of SCI scheme.[30] The 5,15-phenyl substitutions in **Z1** lead to the energy splitting of both Q and B bands while it is more significant for the latter. The present calculation predicts that the low-energy B_y state carries stronger oscillator strength than the high-energy B_x state in agreement with the ab initio SAC-CI calculations.[31] The phenyl substitutions also give rise to the red shift of both Q and B bands; the calculated energy shifts of these absorptions are 0.04 and 0.14 eV, respectively, which are in good agreement with the corresponding experimental values of 0.04 and 0.13 eV. As shown in Table 1, both Q and B states are dominated by transitions within the Gouterman's four orbitals[32] illustrated in Figure 3, while the relatively reduced W_4 values for the B states are due to an admixing of excitation from the lower a_{2u} orbital as has been established to be a common feature of porphyrin compounds by the SAC-CI calculations.[31]

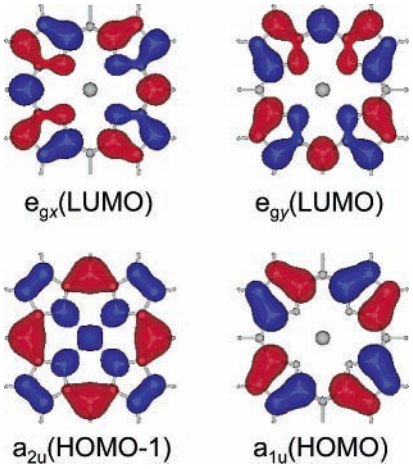

Figure 3. Schematic representation of the frontier four orbitals of Zn^{II}-porphin (**Z1′**).

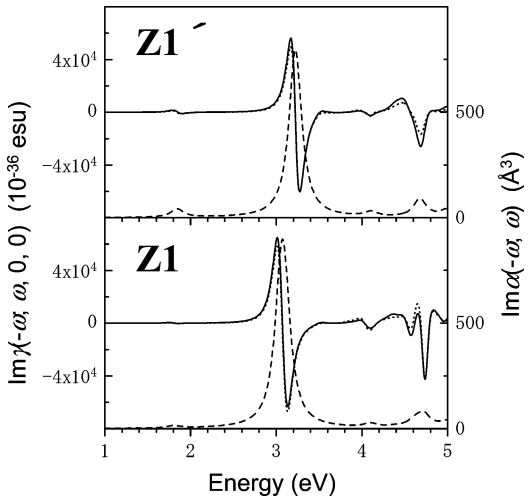

Figure 4. Comparison between the INDO/S-SCI-SOS simulations of the electroabsorption spectra of porphyrin monomers (**Z1′** and **Z1**) obtained (i) by using eqs 2 and 3 (solid lines) and (ii) by using eq 4 including only the $\gamma_{xxxx}/5$, $\gamma_{yyyy}/5$, $\gamma_{xxyy}/15$, and $\gamma_{yyxx}/15$ components (dotted lines). The calculated linear-absorption spectra are shown by dashed lines.

The INDO/S-SCI simulated EA spectra for both **Z1′** and **Z1** are displayed in Figure 4. It is noted that the spectrum calculated by eqs 2 and 3 is sufficiently reproduced by that obtained with eq 4 and including only the four tensor components: $\gamma_{xxxx}/5$, $\gamma_{xxyy}/15$, $\gamma_{yyxx}/15$, and $\gamma_{yyyy}/5$. Since these components represent a response to the static field applied in the molecular plane, this situation is consistent with the two-dimensional π-electron delocalization in porphyrins. Consistent with experiment (Figure 2), the calculated EA spectra exhibit a first-derivative profile

with respect to the B-band absorptions. The analysis of SOS expressions reveals that the quadratic Stark shifts of both B_x and B_y states of **Z1** are caused by their electronic coupling with numerous higher lying (3.8−5.5 eV) two-photon states, consistent with the situation of the Q-band of *meso*-ethynyl attached Zn^{II}-porphyrin as revealed by the INDO/S-MRDCI calculations.[33]

Charge-Transfer (CT) Excited States of Porphyrin Arrays. The transition properties of low-lying electronic excited states for **Z2** ($\theta = 90°$) are listed in Table 2 as obtained by the INDO/S-SCI calculations; the results for **Z2′** obtained by the same method have been reported in ref 7 (in which the B_1 and B_3 representations of the D_2 point group should be interchanged to compare with Table 2). The calculated B-band transition energies are in sufficient agreement with experiments and they are red-shifted relative to those of **Z2′** by 0.09 (B_x) and 0.13 (B_y) eV as a result of *meso*-phenyl substitutions. As shown in Table 2, there are eight charge-transfer (CT) excited states in the energy range spanned by the split B bands. These CT states together with the localized excitations (LE), Q_i and B_i states, form a complete set of 16 eigenstates resulting from one-electron excitations within the eight orbitals which are formed by the four orbitals in each porphyrin unit.[7] As can be seen from their P_{CT} values, the mixing of LE and CT character in the excited states is minimized for **Z2** due to nearly prohibited π-electron delocalization between the porphyrin subunits. For the description of these CT states, it is convenient to utilize the four orbitals localized in each subunit that are basis functions for the C_{2v} subgroup of the D_{2d} point group. In terms of transitions among these MOs, the electronic wave functions of CT states (D_{2d}- and D_2-symmetry adapted form) are represented by

$$\Psi(CT_0,CT_x) = [\Phi(a_{1u}{}^{L}\rightarrow e_{gy}{}^{R}) \pm \Phi(a_{1u}{}^{R}\rightarrow e_{gy}{}^{L})]/2^{1/2} \quad (5)$$

$$\Psi(CT_y,CT_z) = [\Phi(a_{1u}{}^{L}\rightarrow e_{gx}{}^{R}) \pm \Phi(a_{1u}{}^{R}\rightarrow e_{gx}{}^{L})]/2^{1/2} \quad (6)$$

$$\Psi(CT_0{}',CT_x{}') = [\Phi(a_{2u}{}^{L}\rightarrow e_{gx}{}^{R}) \pm \Phi(a_{2u}{}^{R}\rightarrow e_{gx}{}^{L})]/2^{1/2} \quad (7)$$

$$\Psi(CT_y{}',CT_z{}') = [\Phi(a_{2u}{}^{L}\rightarrow e_{gy}{}^{R}) \pm \Phi(a_{2u}{}^{R}\rightarrow e_{gy}{}^{L})]/2^{1/2} \quad (8)$$

where the superscripts L and R denote the left and right subunits, respectively. Note that the net charge transfer (hence, the permanent dipole moment) in these vanishes due to symmetry reasons. Although the $CT_x{}'$ state is dipole forbidden in the D_{2d} system, it becomes allowed via a symmetry lowering into D_2 when $\theta < 90°$. It is noteworthy that for each direction of electron transfer (L → R or R → L), the above four configurations belong to different C_{2v} representations thus prohibiting the configuration interaction among Ψs of eqs 5 to 8. The slight lifting of degeneracy for the CT_0-CT_x pair is due to the indirect π-conjugation,[7] while the degeneracy of the $CT_0{}'-CT_x{}'$ pair is maintained within the π-electron approximation and lifted by the interaction with σ electrons.

Figure 5 shows the energy levels of both CT and B states as a function of intersubunit distance R_{m-m} ($C_{meso}-C_{meso}$ distance) for the system of two orthogonally arranged porphines. As can be seen, the CT levels strongly depend on the intersubunit distance since the Coulomb attraction between electron and hole constitutes an important stabilizing factor.[34] Figure 5 clearly demonstrates that the quasidegeneracy of CT and B bands is quite specific to the directly linked diporphyrins in which the interunit distance is minimized to $R_{m-m} = 1.51$ Å. On the other hand, the interporphyrin distance for some representative *meso*−*meso*-bridged diporphyrins is much longer: $R_{m-m} = 5.843$ Å in the phenyl-bridged diporphyrin (B3LYP/6-31G optimized geometry) and $R_{m-m} = 6.646$ Å in the butadiyne-bridged dimer.[35] Note that the magnitude of Coulomb attraction and hence the energy level of CT states are nearly independent of the mutual orientation of two porphyrin rings if the interunit distance was sufficiently long; actually, for the model system shown in Figure 5, we have confirmed that the CT levels are essentially unchanged even if the two porphines are rearranged into a coplanar orientation at $R_{m-m} \geq 4.0$ Å. Therefore, on the basis of the energy diagram shown in Figure 5, the CT states of the above-mentioned systems are expected to be higher than their B bands, whereas a precise calculation is further required for the butadiyne-bridged dimer since the π-conjugation causes some admixing of CT and LE states. The accidental degeneracy of CT and B bands in the directly linked multiporphyrin systems

TABLE 2: Transition Properties and Electronic Structures of the Lowest 16 Singlet Excited States of Z2 ($\theta = 90°$) As Obtained from INDO/S-SCI Calculations

	state[b]					
band[a]	D_{2d}	D_2	ΔE (eV)[c]	f[d]	P_{CT} (%)[e]	W_8 (%)[f]
Q_x	$1B_2$	$1B_3$	1.77 (2.09)	0.010	1.9	96.5
Q_y	$1E$	$1B_2$	1.77	0.004	1.7	96.4
Q_z	$1E$	$1B_1$	1.78	0.004	1.5	96.4
Q_0	$2A_1$	$2A_1$	1.80	0	1.0	96.5
B_x	$2B_2$	$2B_3$	2.76 (2.75)	3.998	9.7	94.7
CT_y	$2E$	$2B_2$	2.85	0.485	78.0	93.4
CT_z	$2E$	$2B_1$	2.86	0.418	80.4	93.6
$CT_x{}'$	$1A_2$	$3B_3$	2.95	3×10^{-5}	96.3	90.9
$CT_0{}'$	$1B_1$	$3A_1$	2.95	0	96.2	90.9
B_z	$3E$	$3B_1$	3.03 (2.98)	2.060	22.3	93.5
B_y	$3E$	$3B_2$	3.05 (2.98)	2.159	22.7	93.4
CT_0	$3A_1$	$4A_1$	3.08	0	98.2	98.1
CT_x	$3B_2$	$4B_3$	3.13	0.206	90.0	97.6
$CT_y{}'$	$4E$	$4B_2$	3.20	0.067	95.0	97.0
$CT_z{}'$	$4E$	$4B_1$	3.20	0.114	93.5	97.0
B_0	$4A_1$	$5A_1$	3.24	0	1.7	89.4

[a] The subscript indicates the orientation of transition dipole moment (0 for the dipole-forbidden state). [b] The molecular symmetry of **Z2** ($\theta = 90°$) is essentially D_{2d} and its reduction to D_2 is due to the nonorthogonal orientation of peripheral phenyl groups with respect to the porphyrin plane. [c] Excitation energy. The experimental values taken from ref 3 are listed in parentheses. [d] Oscillator strength. [e] Inter-unit charge-transfer probability defined by $P_{CT} = \sum_{I\neq J}\sum_{r\in I}\sum_{s\in J}P_{e-h}(r,s)$, where $I(J)$ represents one porphyrin subunit in a dimer including peripheral phenyl groups. [f] The weight of the transitions within eight orbitals in the SCI wave function.

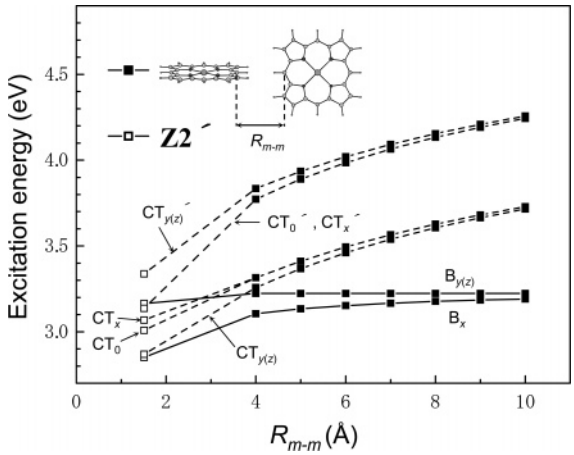

Figure 5. Dependence of the excitation energies of both B and CT states on the interporphyrin distance R_{m-m} ($C_{meso}-C_{meso}$ distance) of orthogonally arranged two Zn^{II}-porphins as obtained by the INDO/S-SCI calculations (filled squares). The excitation energies plotted at $R_{m-m} = 1.51$ Å (open squares) were obtained for **Z2′**.

leads to their unique photophysical properties including the electrooptic response investigated herein.

In Figure 5 the excitation energies obtained for **Z2′** are plotted at $R_{m-m} = 1.51$ Å, which can be compared with those for **Z2** listed in Table 2. It is noted that the *meso*-phenyl substitutions alter the energy levels for the CT_0-CT_x and $CT_0'-CT_x'$ pairs (the latter is located below the former in **Z2**) while the situation for the CT_y-CT_z and $CT_y'-CT_z'$ pairs is not changed. As will be shown later, the close proximity of the CT_0' state to the B_x state is a key factor that provides the characteristic EA spectra of **Z*n*** arrays.

The electronic excited states of **Z3** ($\theta = 90°$) were also calculated by the INDO/S-SCI method (see the Supporting Information). The calculation predicts that the Q_x and B_x bands would be red-shifted by 0.03 and 0.16 eV on going from **Z2** to **Z3** in good agreement with the corresponding experimental values of 0.06 and 0.14 eV, respectively. In the case of a trimer, the charge-transfer transitions between four orbitals on adjacent macrocycles give rise to 16 eigenstates. The wave functions of these CT states are represented in analogy to those of a dimer while each CT state corresponding to eqs 5 to 8 is further classified into two eigenstates. For instance, the CT_0 or CT_x state of the dimer (eq 5) leads to the following two states in the trimer:

$$\Psi(CT_0,CT_x) = [\Phi(a_{1u}{}^{C}\rightarrow e_{gy}{}^{L}) \pm \Phi(a_{1u}{}^{C}\rightarrow e_{gy}{}^{R})]/2^{1/2} \quad (9a)$$

$$\Psi(\underline{CT_0},\underline{CT_x}) = [\Phi(a_{1u}{}^{L}\rightarrow e_{gy}{}^{C}) \pm \Phi(a_{1u}{}^{R}\rightarrow e_{gy}{}^{C})]/2^{1/2} \quad (9b)$$

where the superscripts L, C, and R denote the left, center, and right subunits, respectively, and the configuration interaction between Ψs of eqs 9a and 9b is essentially disrupted due to the orthogonal conformation of neighboring porphyrins. The expressions for the other CT states can be obtained from eqs 6, 7, and 8 in a similar way. In addition to these nearest-neighbor CT states, there are eight CT states associated with transitions between the terminal macrocycles in **Z3**. The present calculation reveals that such CT states are located in the energy region between 3.78 and 3.96 eV, which is consistent with the energy diagram shown in Figure 5 since the *meso*−*meso* distance between the terminal porphyrins amounts to 9.96 Å (B3LYP optimized geometry). We found that these long-range CT states do not contribute to the EA spectrum in the B-band region due to their small transition moments with the B states.

Electroabsorption Spectra of Porphyrin Dimers. We have calculated the EA spectra of *meso*−*meso*-linked diporphyrins (**Z2′** and **Z2**) with $\theta = 90°$ by the INDO/S-SCI SOS method and found that for both systems the EA spectrum calculated by including only the triply resonant SOS terms (eq 4) as well as the γ_{xxxx}, γ_{yyxx}, and γ_{zzxx} components is nearly identical with that obtained by the more complete expressions (eqs 2 and 3). This implies that the modulation spectra of these systems are dominated by a response to the static electric field applied along the *x* axis (the long molecular axis), and hence we focus on the EA spectra calculated by eq 4 to facilitate the analysis of essential excited states responsible for the NLO response of porphyrin arrays. In addition, we refer to the γ tensor components by the following notations: $\gamma_x = \gamma_{xxxx}/5$ and $\gamma_{yz} = (\gamma_{yyxx} + \gamma_{zzxx})/15$.

The calculated EA spectrum of **Z2′** ($\theta = 90°$) is decomposed into the γ_x and γ_{yz} components in Figure 6 (top panel). The contribution from the γ_x component is dominant and its line shape is analogous as a whole to the experimental EA spectrum of **Z2** (Figure 2) in the sense that there are one positive and two negative main peaks in both spectra. However, in the calculated spectrum, the high-energy negative peak is significantly red-shifted relative to the B_{yz} band in contrast to the experimental spectrum indicating that the peripheral phenyl groups should be taken into account for an accurate simulation.

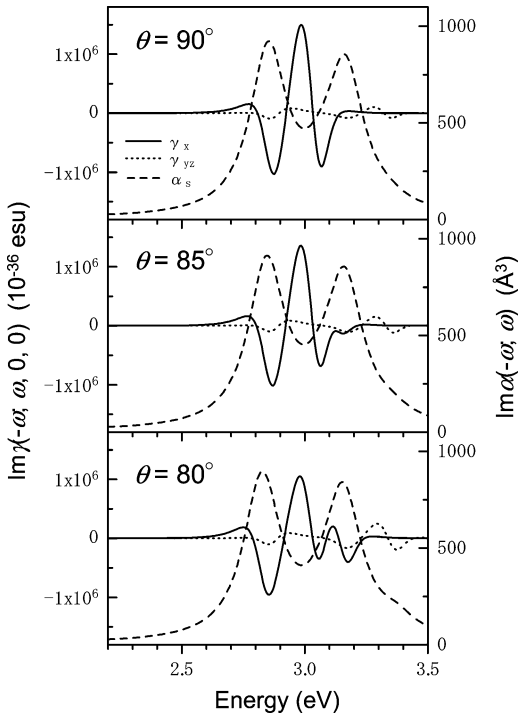

Figure 6. Linear and electroabsorption spectra of **Z2′** with an interporphyrin dihedral angle θ of 90°, 85°, and 80°, as simulated by the INDO/S-SCI-SOS method (eq 4, $\gamma_x \equiv \gamma_{xxxx}/5$, $\gamma_{yz} \equiv (\gamma_{yyxx} + \gamma_{zzxx})/15$).

Therefore, we have calculated also the EA spectrum of **Z2** ($\theta = 90°$). As seen in Figure 7 (top panel), the *meso*-phenyl substitutions lead to a significant enhancement of the γ_{yz} component relative to the γ_x component. But, it is also noteworthy that the single γ_x spectrum sufficiently reproduces the experimental EA spectrum of **Z2**. We found that the relative contribution of the γ_{yz} component becomes larger along with an increasing number of active MOs included in the SCI expansion and this feature does not show any saturation even at the full active space. This implies that the present computation is not stable in this respect, while such a problem was not encountered for **Z2′**. Since the π-conjugation between porphyrin and phenyl groups should not be so significant due to the large dihedral angle between them, the magnitude of the γ_{yz} component would be artificially overestimated by the present computations. Therefore, we focus on the single γ_x spectrum in every system of **Z2** and **Z3** in the following discussions.

At this stage, it would be useful to discuss the precise location of CT states in comparison with the ab initio SAC-CI calculations performed on **Z2′**.[31] This theory predicts that the degenerate CT_y and CT_z states are located 0.13 eV below the B_x state in contrast to the present INDO/S-SCI calculations. In the same reference, the SCI theory is compared with the SAC-CI theory demonstrating that the former tends to overestimate the excitation energies for both CT_y (CT_z) and CT_y' (CT_z') states relative to the B states. Therefore, it is likely that the CT_y and CT_z states are actually located below the B_x state even in **Z2**. Since the negative γ_{yz} peak around the B_x band is due to a resonance to these CT states (Figure 7), this signal should be located in the low-energy side of the B_x band consistent with the experimental

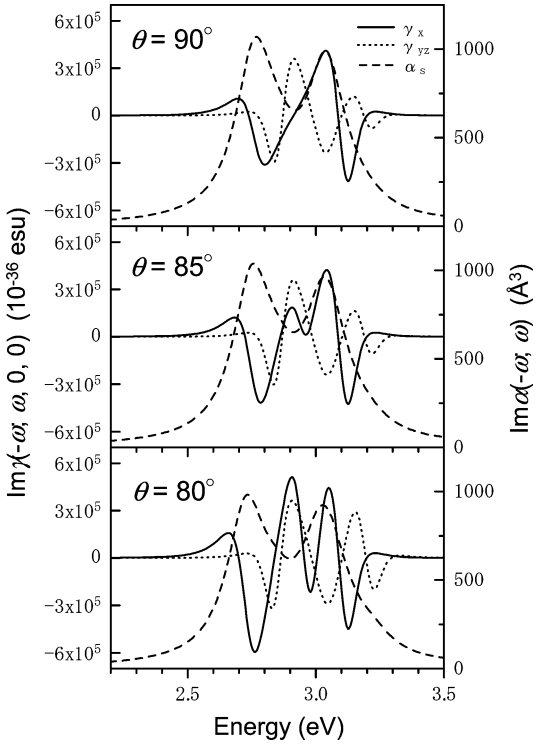

Figure 7. Linear and electroabsorption spectra of **Z2** with an interporphyrin dihedral angle θ of 90°, 85°, and 80°, as simulated by the INDO/S-SCI-SOS method (eq 4, the same definition for the γ_x and γ_{yz} components as in Figure 6). The single γ_x spectrum at $\theta = 90°$ is in excellent agreement with the experimental spectrum of **Z2** (Figure 2) and the γ_{yz} component is likely to be overestimated by the present computations as discussed in the text.

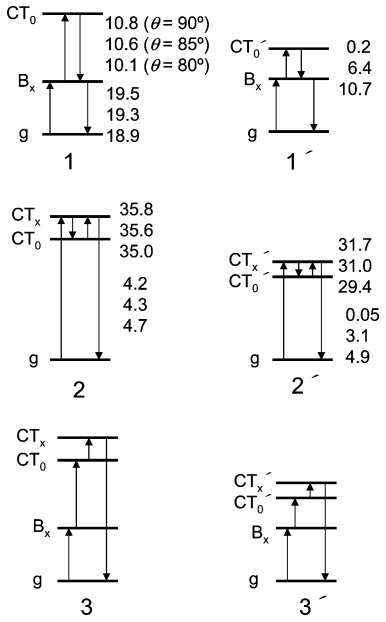

Figure 8. Scheme of the dominant optical channels in the description of the electroabsorption spectrum of **Z2** around its B bands; channel 1 corresponds to the term with $l = B_x$, $m = CT_0$, and $n = B_x$ in eq 4 and so on. The magnitude of transition dipole moment (in Debye units) is also indicated for each transition as obtained by the INDO/S-SCI calculations.

EA spectrum (Figure 2), which exhibits a weak signal below the B_x band (~2.6 eV).

For **Z2**, the dominant optical channels in providing their EA spectrum (γ_x component) are depicted in Figure 8 and the contribution from each channel is shown in Figure 9 (top panel).

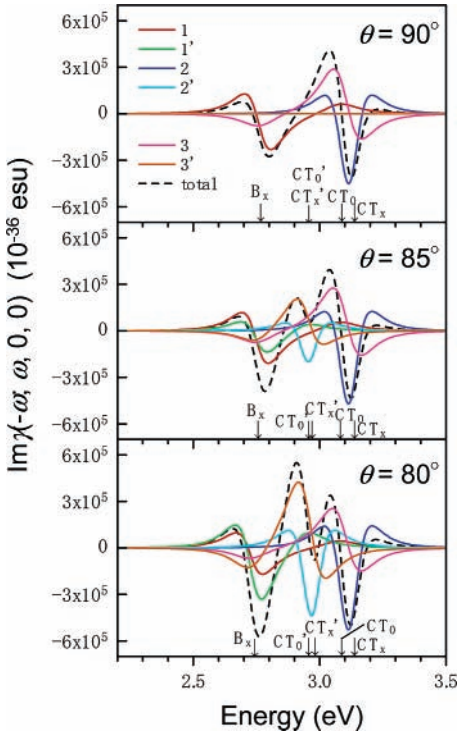

Figure 9. Contribution from each optical channel shown in Figure 8 to the electroabsorption spectrum (γ_x component) of **Z2** as obtained by the INDO/S-SCI-SOS method. The energy levels of essential excited states are indicated by arrows.

Note that the channels 1′, 2′, and 3′ are activated only when $\theta < 90°$ since the relevant transition dipole moments, $\langle B_x|\mu_x|CT_0'\rangle$ and $\langle\gamma|\mu_x|CT_x'\rangle$, vanish at $\theta = 90°$ (essentially the D_{2d} symmetry). Then, the overall EA spectrum of **Z2** arises from the combination of channels 1 and 3 (peaks in the negative region) and channel 2 (positive region) when $\theta = 90°$. As can be seen in Figure 9, the EA signal around the B_x band is mainly due to channel 1, which represents the quadratic Stark shift of the B_x state caused by a coupling with the CT_0 state. We found that the electronic coupling of the B_x state is dominated by the CT_0 state in contrast to the case of **Z1**, while the contributions from higher lying doubly excited states have not been explored within the SCI scheme.

The EA profile associated with the quadratic Stark shift strongly depends on the energy gap Δ between relevant excited states (here, the B_x and CT_0 states) relative to their line widths Γ: a purely first-derivative profile emerges when $\Delta \gg \Gamma$ while the contribution of second-derivative nature increases along with decreasing Δ, and the line shape becomes essentially second derivative when $\Delta \leq \Gamma$.[15,16] Although $\Delta = 0.32$ eV for the B_x and CT_0 states is larger than their line widths of 0.09 eV, we note the rather enhanced second-derivative nature for the channel 1 spectrum as compared with the EA spectrum of **Z1**. It is also noteworthy that the field-induced absorption by the CT_0 state is quite significant in the present system since this state is coupled with two nearby dipole-allowed states (B_x and CT_x) as represented by the channel 2 spectrum. The spectrum of channel 3 exhibits more clear second-derivative profile than that of channel 1 as a result of a much smaller energy gap between the CT_x and CT_0 states ($\Delta = 0.05$ eV), which also allows a triply resonant enhancement of this signal.

The EA signal around the B_{yz} band has been previously assigned as the quadratic Stark shift of the intense B_{yz} band.[10] In contrast, the present calculations reveal that the spectra of channels 2 and 3 merge into the EA signal similar to the first-

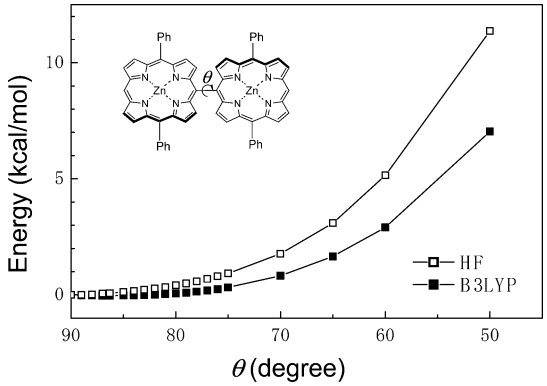

Figure 10. Torsional potential energy curves for **Z2** as obtained by the ab initio HF and the B3LYP calculations.

derivative of the B_{yz} band as a result of the close proximity of both CT_0 and CT_x states to the B_{yz} band. Although the Stark shift of the B_y and B_z states via the coupling with CT_z and CT_y states, respectively, is dominant in the γ_{yz} spectrum of **Z2**, the magnitude of the γ_{yz} component should be much smaller as discussed above and, anyway, this spectrum does not coincide with the experimental spectrum. The Stark shift of the B_y and B_z states via the same mechanism as that of monomer can be roughly estimated from the EA spectrum of **Z1** (Figure 4), which has been obtained with the same line-width parameters as **Z2**. Then, the comparison of Figures 4 and 7 deduces that the EA signal arising from the monomeric Stark shift of the B_{yz} band would be an order of magnitude smaller than the contribution from the CT_0 and CT_x states. In addition, it is noteworthy that the relevant EA signal is gradually red-shifted relative to the B_{yz} band along with an increasing number of porphyrin units (Figure 2) and significantly deviates from the first derivative of the B_{yz} band in much longer arrays (e.g., **Z96**[36]). This feature is not consistent with a simple Stark shift of the B_{yz} band, but can be reproduced by the present calculations on **Z2** and **Z3** as will be shown later.

As displayed in Figure 10, the present B3LYP calculations predict that the torsional potential of **Z2** is rather flat in the range of $\theta = 90-70°$ as in the case of **Z2′**.[7] The full geometry optimization under the D_2-symmetry constraint leads to $\theta = 86.3°$ and the potential energy is raised by merely 0.09 and 0.86 kcal/mol at $\theta = 80°$ and 70°, respectively. However, the applicability of density functional theory (DFT) is rather questionable for determining single-bond torsional potential in π-conjugated systems. It has been pointed out that DFT overestimates the stability of coplanar π-conjugated conformations for the systems such as biphenyl and bithiophene as compared with the conventional Hartree−Fock (HF) and Møller−Plesset second-order perturbation (MP2) theories.[37] Then, we have evaluated the torsional potential of **Z2** also at the HF level on the basis of B3LYP-optimized geometries. As seen in Figure 10, the discrepancy between the HF and B3LYP results becomes more significant for a smaller θ clearly demonstrating the above-mentioned feature of DFT. However, even HF potential is rather flat around $\theta = 90°$ indicating a torsional distribution in the range of $80° \leq \theta \leq 90°$ (the potential minimum at $\theta = 90°$, and 0.12 and 0.41 kcal/mol at $\theta = 85°$ and 80°, respectively).

On the basis of these considerations, we have further calculated the EA spectrum of **Z2** for $\theta = 85°$ and 80° as depicted in Figure 7 in which we again focus on the γ_x components due to the above-mentioned reasons; actually, only the γ_x spectrum is affected by the dihedral angle. Along with decreasing θ, the negative peak at the B_x band is gradually intensified and a new positive signal appears just above it (∼2.9 eV), while there is no significant change in the B_{yz}-band region. Although the experimental spectrum of **Z2** (Figure 2) exhibits a weak feature just above the B_x band (∼2.8 eV), which is consistent with the theoretical prediction, it is almost identical with the theoretical spectrum at $\theta = 90°$ indicating that the mean torsional deformation is minimized for **Z2**. We expect that the torsional deformation would be more significant in longer arrays due to a steric confinement imposed by the surrounding PMMA. In this regard, it is noteworthy that the EA spectra of **Z2** calculated at $\theta = 85°$ and 80° are similar as a whole to the experimental spectra of **Z3** and **Z4**, respectively.

To elucidate the origin of these spectral changes, we performed the same analysis as in the case of $\theta = 90°$. As seen in Figure 9, the spectral change is caused by the contributions from channels 1′, 2′, and 3′ which are activated via the symmetry reduction from D_{2d} to D_2. The magnitude of $\langle B_x|\mu_x|CT_0'\rangle$ which is relevant to both channels 1′ and 3′ rapidly increases even under a slight deviation of θ from 90° (Figure 8). At $\theta = 80°$, the spectrum of channel 1′ exhibits a more significant second-derivative nature and provides a larger negative contribution than that of channel 1. This feature results from the fact that the B_x state is much closer to the CT_0' state ($\Delta = 0.22$ eV) than the CT_0 state ($\Delta = 0.35$ eV) as established by the *meso*-phenyl substitutions. In contrast, as shown in Figure 6, the γ_x spectrum of **Z2′** is essentially unchanged in the B_x-band region even at $\theta = 80°$ due to the larger energy gap between the B_x and CT_0' states ($\Delta = 0.31$ eV; the CT_0' state is located above the CT_0 state in **Z2′**). Therefore, it can be said that the *meso*-phenyl groups of **Z2** are responsible for the sensitivity of its EA spectrum to the dihedral angle.

At this stage, it is worth stressing that although the six channels shown in Figure 8 play a central role in providing the EA spectrum (i.e., the resonant γ) of **Z2**, their overall contribution to the off-resonant γ is quite small due to the cancellation of positive contributions from channels 1 and 2 and the negative one from channel 3. This implies that the interporphyrinic CT states do not contribute to the off-resonant γ of **Z2**, and hence, it should be given by a summation of γ associated with each porphyrin subunit as can be expected from the nearly disrupted interunit π-conjugation. Moreover, since a similar cancellation occurs for channels 1′, 2′, and 3′, the off-resonant γ value of **Z2** should be nearly constant under a slight torsional deformation ($\theta \sim 80°$).

Electroabsorption Spectra of Porphyrin Trimers. The EA spectra calculated for **Z3** with the dihedral angle θ of 90° and 83° are displayed in Figure 11 (only γ_x components are shown due to the above-mentioned reasons). In contrast to the case of **Z2**, the calculated EA spectrum for $\theta = 83°$ is in better agreement with the experimental spectrum than that for $\theta = 90°$ indicating that the mean torsional deformation would be more significant for **Z3** than **Z2**. It is likely that as the length of the porphyrin array increased, the torsional deformation would be more readily introduced via a steric confinement imposed by the surrounding PMMA polymer. The underlying mechanism that accounts for the characteristic EA spectrum at $\theta = 83°$ is similar to that elucidated for **Z2**: the EA signal between 2.5 and 2.8 eV is mainly due to channels 1′ and 3′ involving both B_x and CT_0' states. We note that the energy gap between the B_x-band maximum and the positive EA peak at 2.8 eV is larger than the corresponding experimental value by ca. 0.1 eV. The position of this EA peak depends on that of the CT_0' state and the EA feature around 2.9 eV is due to the induced absorption of the $\underline{CT_0'}$ state. Therefore, we obtain a better simulation

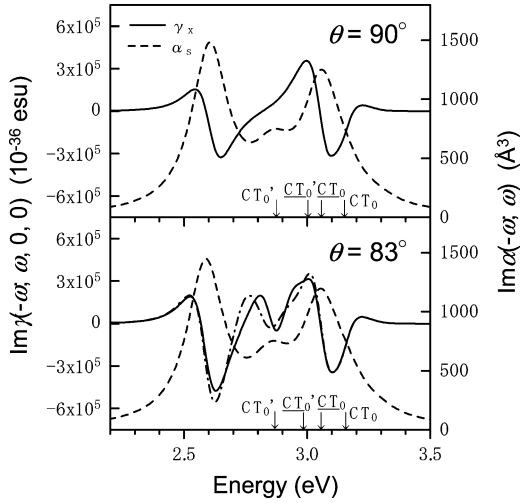

Figure 11. Linear and electroabsorption spectra of **Z3** with an interporphyrin dihedral angle θ of 90° and 83°, as simulated by the INDO/S-SCI-SOS method (eq 4, the same definition for the γ_x component as in Figure 6). The energy levels of CT states that are coupled with the B_x state are indicated by arrows. In the bottom panel ($\theta = 83°$), the γ_x spectrum shown by a dash−dotted line was obtained with the excitation energies for both CT_0' and CT_0' states reduced by 0.1 eV.

regarding these EA profiles when both CT_0' and $\underline{CT_0}'$ states are low-energy shifted by 0.1 eV as shown by the dash−dotted line in Figure 11. Such correction for the CT level is rationalized by the fact that the electronic polarization of PMMA should lead to a larger stabilization for the charge-transfer excitation than the localized one (B_x).[38,28] Note that we consider here an isotropic solvation that maintains the symmetric electronic structure of porphyrin arrays and does not resolve the discrepancy with experiment regarding the position of the negative EA peak relative to the B_x-band maximum. The influence of an anisotropic solvation will be discussed below in relation to this problem.

As for the EA spectrum in the B_{yz}-band region, the calculated spectrum is red-shifted relative to the linear absorption band as compared with the case of **Z2**, which is consistent with the experimental spectra and hence supports the assignment of this signal described above (the superimposition of channels 2 and 3).

In the experimental EA spectra of ***Zn***, the negative peak at the B_x band is remarkably intensified relative to that near the B_{yz} band as the number of porphyrin units increases in the arrays. This feature is partly ascribed to the enhanced torsional deformation in longer arrays based on the computational results shown in Figures 7 and 11. However, it is also noteworthy that both Q(1,0) and B_x bands become sharper along with an increasing number of porphyrin units[4,39] consistent with the view of the electronic transitions of porphyrin *J*-aggregates. The EA intensity depends on the line width, Γ, with Γ^{-2} scaling of features due to the quadratic Stark shift (first-derivative profile) and Γ^{-3} scaling for the quadratic Stark broadening (second-derivative profile).[15,16] Taking account of such strong line width dependence, it is likely that the motional narrowing of the B_x band is predominant in providing the above-mentioned feature of the EA spectra of porphyrin arrays.

Influence of Solvent-Induced Asymmetry and Other Factors. At this stage, it is noteworthy that the second-derivative nature of the EA spectrum at the B_x band is more remarkable in the experiment than the theory; the negative EA peak is located at almost the same energy as the B_x band in the experimental spectra (Figure 2), whereas the corresponding peak is slightly blue-shifted in the calculated spectra of both **Z2** and **Z3** (Figures 7 and 11). This discrepancy might be attributed to a nonzero dipole moment of porphyrin arrays due to an asymmetry induced by the surrounding PMMA, and hence, a contribution from the $\Delta\mu$ channel ($g \rightarrow B_x \rightarrow B_x \rightarrow B_x \rightarrow g$, eq 4) to the EA spectrum. Since the EA spectrum of **Z1** exhibits a predominantly first-derivative line shape even in a PMMA film, the induced dipole moment should be related to an interporphyrinic charge transfer. As described above, the excitonic B_x state is strongly coupled with the nearby located charge-transfer states, CT_0 and CT_0', via the transition dipole moment parallel to the long molecular axis (*x* axis) of the porphyrin array. Then, an asymmetry along the *x* axis allows these CT states to carry net transfer of charge and to admix with the B_x state.

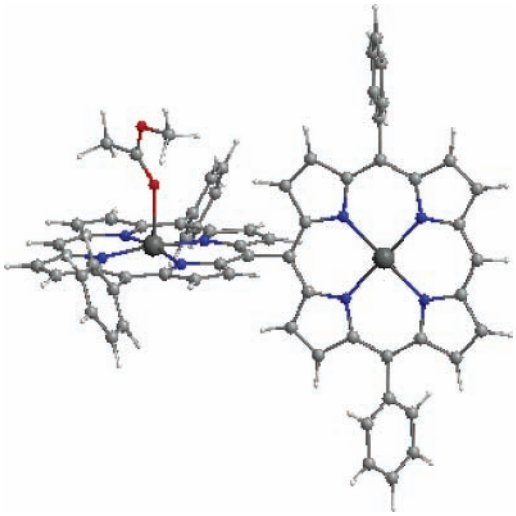

Figure 12. B3LYP/6-31G optimized structure of a 1:1 complex of **Z2** and methyl acetate (a model for the side chain of PMMA).

Although we do not have any precise knowledge of nanoenvironmental structure, it is likely that the ester side group of PMMA (Figure 1) adsorbs on the positively charged Zn^{II}-center of porphyrin and an asymmetric situation for **Z2** is established, for instance, as shown in Figure 12 (the side group of PMMA is modeled by a methyl acetate). The geometry of this complex was fully optimized at the B3LYP level and the adsorption energy of methyl acetate was found to be 8.7 kcal/mol. Due to the C_1 symmetry of this complex, we were forced to reduce the number of active MOs from 360 (all valence MOs) to 248 in the SCI expansion, while the check performed on the unperturbed **Z2** revealed that such truncation would not affect the essential points described below. The SOS-simulated EA spectrum is depicted in Figure 13 in which we focus on the γ_x component as in the case of unperturbed systems. It is noted that the magnitude of $\Delta\mu_x$ for the B_x state amounts to 12.7 D and it leads to a significant contribution from the $\Delta\mu$ channel involving the B_x state. However, the EA spectrum of this complex is in less agreement as a whole with the experiment than that of the unperturbed **Z2** (top panel of Figure 7). The energy level of essential CT states, CT_0 and CT_0', is indicated in Figure 13. These CT states are now characterized as a one-way electron transfer from the adsorbed porphyrin to the free one and they are remarkably stabilized with respect to the B bands as compared with the unperturbed system. The unique EA signal just below the B_x band arises from several channels involving the CT_0' state which are activated by the torsional deformation. The red-shift of the CT_0 state leads to that of the

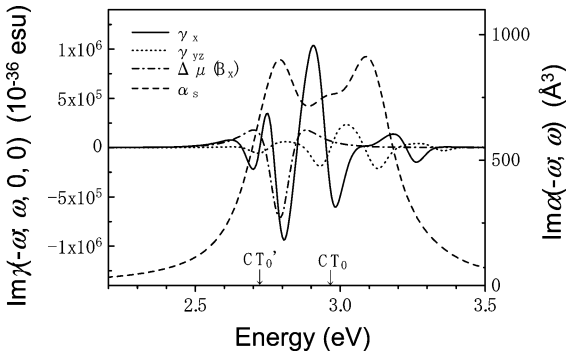

Figure 13. INDO/S-SCI-SOS simulated linear and electroabsorption spectra for the complex shown in Figure 12. The contribution of the $\Delta\mu(B_x)$ channel ($g \rightarrow B_x \rightarrow B_x \rightarrow B_x \rightarrow g$) is shown by a dash−dotted line and the energy levels of the CT_0 and CT_0' states are indicated by arrows.

high-energy EA signal relative to the B_{yz} band, while the corresponding EA signal is overlapping with the B_{yz} band in both the experimental spectrum and the theoretical spectrum of unperturbed **Z2**. Therefore, it is expected that the PMMA coordination would not be a major situation for the porphyrin arrays occurring in the actual sample. Moreover, we have examined the influence of anisotropic local field as represented by a uniform static field applied along the *x* axis and found a red-shift of the EA signal around the B_{yz} band similar to the above-mentioned case.

On the other hand, we should take account of the vibronic coupling between the Q and B_x states as well as the summation over the vibrational levels in the SOS simulation of EA spectrum. It is well-known that the Q(1,0) bands of Zn^{II}-porphyrins gain their intensities via vibronic coupling from the B bands. Since the vibronic coupling causes an admixing of the electronic nature of the B_x state into the Q states, it is likely that the transition dipole moments between the Q states and both CT_0 and CT_0' states are also enhanced. Because the optical channels $g \rightarrow Q \rightarrow CT_0$ (CT_0') $\rightarrow B_x \rightarrow g$ would give rise to a breaching at the B_x band similarly to the channels 3 and 3′ (Figure 9), the enhanced contributions from these channels might be responsible for the prominent second-derivative nature observed for the EA spectra of porphyrin arrays. The enhanced Q(1,0) bands of the porphyrin arrays are probably due to the increased vibronic coupling mainly attributed to the decreased energy gap between the B_x and Q bands in porphyrin arrays.[39] Therefore, the effects of vibronic coupling will become more significant also for the EA spectrum as the number of porphyrin units increases. Although the qualitative analysis of vibronic coupling has been successfully performed on the fused porphyrin dimer,[9] the quantitative prediction is unfortunately out of our reach due to intrinsic difficulties involved in the calculation of large macromolecules.

Finally, it is also worthwhile to consider the influence of the *meso*−*meso* dihedral angle (θ) distribution in the actual sample. As shown in Figure 7, the B_x band and the corresponding negative EA peak are gradually red-shifted along with decreasing θ. Following this change, the intensity of the B_x band is slightly reduced whereas the EA signal is remarkably intensified via the activation of the B_x-CT_0' coupling (Figures 8 and 9). Therefore, the EA response would be dominated by those components having θ rather smaller than the average, which leads to an apparent red-shift of the EA signal relative to the B_x band successfully accounting for the discrepancy between the experimental EA spectra and the theoretical ones obtained for each θ. We note that the effect of dihedral angle distribution for porphyrin arrays is in analogy to that of conjugation length distribution for π-conjugated polymers: the latter leads to a red-shift of the EA relative to the linear absorption because EA preferentially probes the longer chain lengths due to their larger exciton polarizability[12] (for the present systems, the polarizability of B_x increases as θ decreases). A detailed analysis of the experimental spectra as in ref 12 taking account of torsional distribution and the results of the present study would be useful for a deeper understanding of the unique NLO response of porphyrin arrays.

IV. Conclusions

The origin of the anomalous EA spectra of directly *meso*−*meso*-linked porphyrin arrays has been investigated by means of the SOS approach at the INDO/S-SCI level. In these systems, the interporphyrinic charge-transfer (CT) excited states are accidentally overlapping with the B bands as a result of close proximity of adjacent porphyrin units. The present calculation reveals that the exciton-split B_x state is strongly coupled via a transition dipole moment with such CT states (CT_0 and CT_0') and the anomalous second-derivative EA shape observed at the B_x band can be mainly attributed to the quadratic Stark effect that is intermediate between Stark shift (first derivative) and Stark broadening (second derivative). Moreover, both intensity and profile of this EA signal are quite sensitive to the dihedral angle (θ) between neighboring porphyrin planes due to the fact that the $B_x \rightarrow CT_0'$ transition dipole moment vanished when $\theta = 90°$ but rapidly increased even under a slight deviation of θ from 90°. The comparison of theoretical and experimental EA spectra suggests that the mean torsional deformation would be more significant for the longer arrays than the dimer when they are doped into a PMMA film.

Since the situation of overlapping LE and CT states is anticipated for other macromolecules that are comprised of mutually orthogonal directly linked conjugated pigments such as bianthryl,[40,41] a similar EA spectrum mediated by the Stark effect close to Stark broadening might be observed for these systems. It is hoped that the underlying mechanism elucidated by the present study for the unique EA spectra of porphyrin arrays would be useful for understanding and controlling the NLO properties of such multichromophoric arrays.

Acknowledgment. The work at Kyoto was supported by Grants-in-Aid for Scientific Research (No.12874076, No. 12440196, and No. 11223205) from the Ministry of Education, Science, Sports and Culture of Japan, and by CREST (Core Research for Evolutional Science and Technology) of Japan Science and Technology Corporation (JST). The work at Hokkaido University was supported by Grants-in-Aid for Scientific Research (A) (2) (15205001) and for Scientific Research on Priority Area (417) from the Ministry of Education, Culture, Sports, Science and Technology of Japan. K.T. acknowledges the support by a Grant-in-Aid for Scientific Research (No. 16350100) from the Ministry of Education, Science, Sports and Culture of Japan.

Supporting Information Available: A table of calculated transition properties and electronic structures of the singlet excited states of **Z3** ($\theta = 90°$). This material is available free of charge via the Internet at http://pubs.acs.org.

References and Notes

(1) (a) Wasielewski, M. R. *Chem. Rev.* **1992**, *92*, 435. (b) Osuka, A.; Mataga, N.; Okada, T. *Pure Appl. Chem.* **1997**, *69*, 797. (c) Nakano, A.;

Osuka, A.; Yamazaki, I.; Yamazaki, T.; Nishimura, Y. *Angew. Chem., Int. Ed. Engl.* **1998**, *37*, 3023. (d) Choi, M.-S.; Aida, T.; Yamazaki, T.; Yamazaki, I. *Angew. Chem., Int. Ed. Engl.* **2001**, *40*, 3194. (e) Takahashi, R.; Kobuke, Y. *J. Am. Chem. Soc.* **2003**, *125*, 2372.

(2) (a) Anderson, H. L. *Chem. Commun.* **1999**, 2323. (b) Kim, D.; Osuka, A. *J. Phys. Chem. A* **2003**, *107*, 8791.

(3) Osuka, A.; Shimidzu, H. *Angew. Chem., Int. Ed. Engl.* **1997**, *36*, 135.

(4) Aratani, N.; Osuka, A.; Kim, Y. H.; Jeong, D. H.; Kim, D. *Angew. Chem., Int. Ed. Engl.* **2000**, *39*, 1458.

(5) Kasha, M.; Rawls, H. R.; El-Bayoumi, M. A. *Pure Appl. Chem.* **1965**, *11*, 371.

(6) Aratani, N.; Cho, H. S.; Ahn, T. K.; Cho, S,; Kim, D.; Sumi, H.; Osuka, A. *J. Am. Chem. Soc.* **2003**, *125*, 9668.

(7) Yoshida, N.; Ishizuka, T.; Osuka, A.; Jeong, D. H.; Cho, H. S.; Kim, D.; Matsuzaki, Y.; Tanaka, K.; Nogami, A.; Tanaka, K. *Chem. Eur. J.* **2003**, *9*, 58.

(8) Cho, H. S.; Jeong, D. H.; Cho, S.; Kim, D.; Matsuzaki, Y.; Tanaka, K.; Tsuda, A.; Osuka, A. *J. Am. Chem. Soc.* **2002**, *124*, 14642.

(9) Jeong, D. H.; Jang, S. M.; Hwang, I.-W.; Kim, D.; Matsuzaki, Y.; Tanaka, K.; Tsuda, A.; Nakamura, T.; Osuka, A. *J. Chem. Phys.* **2003**, *119*, 5237.

(10) Ohta, N.; Iwaki, Y.; Ito, T.; Yamazaki, I.; Osuka, A. *J. Phys. Chem. B* **1999**, *103*, 11242.

(11) Bublitz, G. U.; Boxer, S. G. *Annu. Rev. Phys. Chem.* **1997**, *48*, 213.

(12) Liess, M.; Jeglinski, S.; Vardeny, Z. V.; Ozaki, M.; Yoshino, K.; Ding, Y.; Barton, T. *Phys. Rev. B* **1997**, *56*, 15712.

(13) Phillips, S. D.; Worland, R.; Yu, G.; Hagler, T.; Freedman, R.; Cao, Y.; Yoon, V.; Chiang, J.; Walker, W. C.; Heeger, A. J. *Phys, Rev. B* **1989**, *40*, 9751.

(14) Horvath, A.; Weiser, G.; Baker, G. L.; Etemad, S. *Phys, Rev. B* **1995**, *51*, 2751.

(15) Soos, Z. G.; Mukhopadhyay, D.; Hennessy, M. H. *Chem. Phys.* **1996**, *210*, 249.

(16) Kulakov, T. A.; Paraschuk, D. Y. *Chem. Phys. Lett.* **2000**, *325*, 517.

(17) Frisch, M. J.; Trucks, G. W.; Schlegel, H. B.; Scuseria, G. E.; Robb, M. A.; Cheeseman, J. R.; Zakrzewski, V. G.; Montgomery, J. A.; Stratmann, R. E.; Burant, J. C.; Dapprich, S.; Millam, J. M.; Daniels, A. D.; Kudin, K. N.; Strain, M. C.; Farkas, O.; Tomasi, J.; Barone, V.; Cossi, M.; Cammi, R.; Mennucci, B.; Pomelli, C.; Adamo, C.; Clifford, S.; Ochterski, J.; Petersson, G. A.; Ayala, P. Y.; Cui, Q.; Morokuma, K.; Malick, D. K.; Rabuck, A. D.; Raghavachari, K.; Foresman, J. B.; Cioslowski, J.; Ortiz, J. V.; Baboul, A. G.; Stefanov, B. B.; Liu, G.; Liashenko, A.; Piskorz, P.; Komaromi, I.; Gomperts, R.; Martin, R. L.; Fox, D. J.; Keith, T.; Al-Laham, M. A.; Peng, C. Y.; Nanayakkara, A.; Gonzalez, C.; Challacombe, M.; Gill, P. M. W.; Johnson, B.; Chen, W.; Wong, M. W.; Andres, J. L.; Gonzalez, C.; Head-Gordon, M.; Replogle, E. S.; Pople, J. A. *Gaussian 98*, revision, A.7; Gaussian, Inc.: Pittsburgh, PA, 1998.

(18) Ditchfield, R.; Hehre, W. J.; Pople, J. A. *J. Chem. Phys.* **1971**, *54*, 724.

(19) Huzinaga, S.; Andzelm, J.; Klobukowski, M.; Radzio-Andzelm, E.; Sakai, Y.; Tatewaki, H. *Gaussian Basis Sets for Molecular Calculations*; Elsevier: New York, 1984.

(20) Aratani, N.; Osuka, A. Unpublished work.

(21) Ridley, J. E.; Zerner, M. C. *Theor. Chim. Acta* **1973**, *32*, 111.

(22) Nishimoto, K.; Mataga, N. *Z. Phys. Chem.* **1957**, *12*, 335.

(23) Mukamel, S.; Tretiak, S.; Wagersreiter, T.; Chernyak, V. *Science* **1997**, *277*, 781.

(24) Orr, B. J.; Ward, J. F. *Mol. Phys.* **1971**, *20*, 513.

(25) (a) Shuai, Z.; Brédas, J. L. *Phys. Rev. B* **1991**, *44*, 5962. (b) Shuai, Z.; Brédas, J. L. *Phys. Rev. B* **2000**, *62*, 15452.

(26) Yaron, D.; Silbey, R. *Phys. Rev. B* **1992**, *45*, 11655.

(27) Abe, S.; Schreiber, M.; Su, W. P.; Yu, J. *Phys. Rev. B* **1992**, *45*, 9432.

(28) Beljonne, D.; Shuai, Z.; Cornil, J.; dos Santos, D. A.; Brédas, J. L. *J. Chem. Phys.* **1999**, *111*, 2829.

(29) Sekino, H.; Kobayashi, H. *J. Chem. Phys.* **1987**, *86*, 5045.

(30) Baker, J. D.; Zerner, M. C. *Chem. Phys. Lett.* **1990**, *175*, 192.

(31) Miyahara, T.; Nakatsuji, H.; Hasegawa, J.; Osuka, A.; Aratani, N.; Tsuda, A. *J. Chem. Phys.* **2002**, *117*, 11196.

(32) Gouterman, M. *J. Chem. Phys.* **1959**, *30*, 1139.

(33) Beljonne, D.; O'Keefe, G. E.; Hamer, P. J.; Friend, R. H.; Anderson, H. L.; Brédas, J. L. *J. Chem. Phys.* **1997**, *106*, 9439.

(34) Bilsel, O.; Rodriguez, J.; Milam, S. N.; Gorlin, P. A.; Girolami, G. S.; Suslick, K. S.; Holten, D. *J. Am. Chem. Soc.* **1992**, *114*, 6528.

(35) Taylor, P. N.; Huuskonen, J.; Rumbles, G.; Aplin, R. T.; Williams, E.; Anderson, H. L. *Chem. Commun.* **1998**, 909.

(36) Iwaki, Y.; Ohta, N.; Aratani, N.; Osuka, A. Submitted for publication.

(37) Karpfen, A.; Choi, C. H.; Kertesz, M. *J. Phys. Chem. A* **1997**, *101*, 7426.

(38) (a) Moore, E. E.; Gherman, B.; Yaron, D. *J. Chem. Phys.* **1997**, *106*, 4216. (b) Moore, E. E.; Yaron, D. *J. Chem. Phys.* **1998**, *109*, 6147.

(39) Kim, Y. H.; Jeong, D. H.; Kim, D.; Jeoung, S. C.; Cho, H. S.; Kim, S. K.; Aratani, N.; Osuka, A. *J. Am. Chem. Soc.* **2001**, *123*, 76.

(40) Nakashima, N.; Murakawa, M.; Mataga, N. *Bull. Chem. Soc. Jpn.* **1976**, *49*, 854.

(41) Kajimoto, O.; Yamasaki, K.; Arita, K.; Hara, K. *Chem. Phys. Lett.* **1986**, *125*, 184.